HOKKAIDO UNIVERSITY

Title	Imaging acoustic waves in microscopic wedges
Author(s)	Tomoda, Motonobu; Matsueda, Shinnosuke; Otsuka, Paul H. et al.
Citation	New Journal of Physics, 16(10), 103029 https://doi.org/10.1088/1367-2630/16/10/103029
Issue Date	2014-10
Doc URL	https://hdl.handle.net/2115/57646
Rights(URL)	https://creativecommons.org/licenses/by/3.0/
Type	journal article
File Information	1367-2630_16_10_103029.pdf



Hokkaido University Collection of Scholarly and Academic Papers : HUSCAP

IOPscience iopscience.iop.org

Home Search Collections Journals About Contact us My IOPscience

Imaging acoustic waves in microscopic wedges

This content has been downloaded from IOPscience. Please scroll down to see the full text.

2014 New J. Phys. 16 103029

(http://iopscience.iop.org/1367-2630/16/10/103029)

View the table of contents for this issue, or go to the journal homepage for more

Download details:

IP Address: 133.87.166.83
This content was downloaded on 06/01/2015 at 04:41

Please note that terms and conditions apply.

New Journal of Physics
The open access journal at the forefront of physics
Deutsche Physikalische Gesellschaft DPG | IOP Institute of Physics

Imaging acoustic waves in microscopic wedges

Motonobu Tomoda[1], Shinnosuke Matsueda[1], Paul H Otsuka[1], Osamu Matsuda[1], Istvan A Veres[2], Vitalyi E Gusev[3] and Oliver B Wright[1]

[1] Division of Applied Physics, Faculty of Engineering, Hokkaido University, Sapporo, 060-8628, Japan
[2] Research Center for Non-Destructive Testing GmbH, Altenberger Str. 69, 4040 Linz, Austria
[3] LUNAM Université, Université du Maine, CNRS, LAUM UMR 6613, Avenue Olivier Messiaen, Le Mans 72085, France
E-mail: mtomoda@eng.hokudai.ac.jp

Received 20 June 2014, revised 19 August 2014
Accepted for publication 1 September 2014
Published 16 October 2014
New Journal of Physics **16** (2014) 103029
doi:10.1088/1367-2630/16/10/103029

Abstract

Using an ultrafast optical technique we image near-gigahertz flexural acoustic waves propagating in a thin gold wedge deposited on an ultrathin silicon nitride slab. Temporal Fourier transforms of the imaged data in two dimensions allow individual frequencies to be accessed. The wave fronts associated with antisymmetric Lamb waves bend towards the thin end of the wedge. This behaviour is mimicked with an analytical model based on sections of a linear wedge. We also conduct numerical simulations which show good agreement with the experimental results.

S Online supplementary data available from stacks.iop.org/njp/16/103029/mmedia

Keywords: wedge, Lamb waves, acoustics, imaging, ultrafast

1. Introduction

Acoustic waves of various kinds in wedges (Lagasse *et al* 1973, De Billy and Hladky-Hennion 1999, Shuvalov and Krylov 2000, Yang and Tsen 2006, Moss *et al* 1973, Krylov 1998, Lomonosov *et al* 2012) have spurred a great deal of research. Such research can also be applied to, for example, ultrasonic transducers (Bertoni and Tamir 1975, Manneberg *et al* 2008), vibration damping (Bayod 2011, Bowyer *et al* 2012), nondestructive testing of

Content from this work may be used under the terms of the Creative Commons Attribution 3.0 licence. Any further distribution of this work must maintain attribution to the author(s) and the title of the work, journal citation and DOI.

© 2014 IOP Publishing Ltd and Deutsche Physikalische Gesellschaft

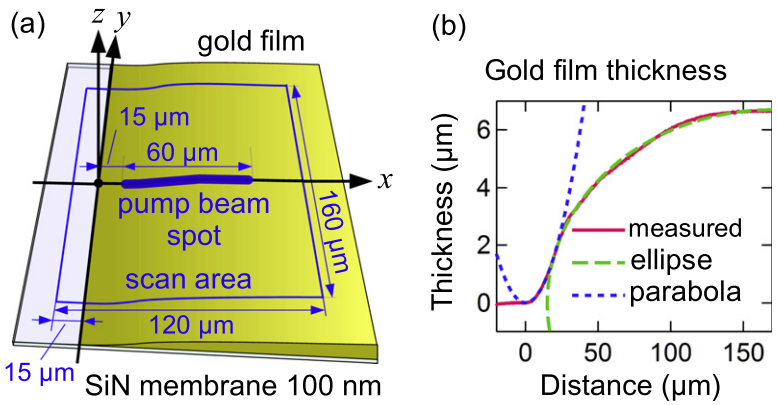


Figure 1. (a) Schematic of sample structure and imaged region. (b) Thickness of gold film measured by a confocal laser scanning microscope (solid red line). The gold film thickness variation is fitted with parabolic (dotted blue line) and ellipsoidal (dashed green line) functions for semi-analytical and numerical modeling.

blades (Joosse *et al* 2002, Liu and Yang 2010), moisture detection (Tung and Yang 2010), black-hole analogies (Krylov and Tilman 2004, Krylov and Winward 2007), and even aquatic propulsion (Krylov and Pritchard 2007). Various kinds of acoustic modes are known to exist in wedges. Acoustic waves may, for example, be guided along the thin edge of a wedge. For perfect wedges with sharp edges—there being no characteristic length scale in this case—such waves are non-dispersive (Moss *et al* 1973, Jia and De Billy 1992). In contrast, waves launched from inside the wedge towards the thin edge are highly dispersive and show a steadily decreasing sound velocity as they travel (Krylov and Tilman 2004). Plane waves launched from inside the wedge parallel to the edge of the wedge are therefore expected to follow curved ray paths (Shuvalov and Krylov 2000). Although laser ultrasonics had been used to generate and detect the waves in wedges for years (Hess *et al* 2014, Jia and De Billy 1992, Jia *et al* 2011, Edwards *et al* 2012), to our knowledge there has been no attempt to image them at near-gigahertz frequencies or at micron lateral resolution.

In this paper we use an ultrafast optical technique to excite and to image near-gigahertz flexural acoustic waves in gold wedges deposited on thin silicon nitride slabs. The optical pulses are focused to a line source set perpendicular to the edge of the wedge. The wave propagation characteristics are imaged in the time domain by using scanned optical probing. By using temporal Fourier transforms, we extract constant-frequency images, also viewable as animations, and observe wave-front bending. This behaviour is explained with the help of a semi-analytical model based on the theory of flexural waves in a double-film layer.

2. Sample and method

A microscopic gold wedge was prepared by radio-frequency (rf) sputtering, making use of a programmable translation stage inside the vacuum chamber with a 0.5 μm positioning accuracy. The schematic of the sample structure is shown in figure 1(a). During the rf sputtering at a constant deposition rate of 0.4 nm s^{-1}, a thin flat mask plate attached to the translation stage is moved just above the substrate surface in the $-x$ direction (see figure 1). The substrate is a commercial amorphous-SiN slab with a thickness of 100 nm. The spatial thickness distribution

of the gold wedge was mapped by a confocal laser-scanning microscope, and the profile is shown in figure 1(b). The wedge thickness changes along the x-axis from 0 to 6 μm over a $\sim$150 μm distance. Local thickness variations along the y-direction are within 10 nm over the imaged region.

The acoustic wave field is imaged by the use of an optical pump-and-probe technique combined with a common-path interferometer (Sugawara *et al* 2002, Tachizaki *et al* 2006). The pump (frequency-doubled, wavelength 415 nm, incident pulse energy 0.18 nJ) and probe (wavelength 830 nm, incident pulse energy 0.06 nJ) pulses originate from a mode-locked Ti: Sapphire laser with an 80.4 MHz repetition rate and a 0.2 ps pulse duration. The pump pulses, frequency-doubled by a BBO (β-BaB_2O_4) crystal, modulated at 1 MHz for lock-in detection, reshaped by a cylindrical lens and a ×50 microscope objective lens, produce a quasi-line source with $\sim$60 μm length and $\sim$2 μm width (full width at half maximum) on the sample surface. The line source is perpendicular to the edge of the wedge, and the line centre is set at a distance of 45 μm from the edge (figure 1(a)). Broadband plane Lamb waves including both quasi-symmetric and quasi-antisymmetric modes with near-GHz frequencies are thermoelastically generated. (Because of the presence of the thin silicon nitride slab, perfectly symmetric or anti-symmetric modes do not exist.) Out-of-plane motion ($\sim$10 pm in amplitude) is detected with $\sim$0.5 pm resolution by two probe pulses at an interval of 300 ps, using MHz lock-in detection at the frequency of the pump-beam chopping. The 2 μm diameter probe spot is scanned over a 120 μm × 160 μm region including the edge of the wedge, as shown in figure 1(a), and the optical phase difference $\Delta\phi$ between the probe pulses is imaged at a fixed pump-probe delay time τ. Here $\Delta\phi \propto du_z/dt$, the time derivative of the out-of-plane motion. By incrementing τ, animations of 24 frames are obtained within the 12.44 ns laser repetition period at 0.52 ns intervals.

To model and simulate the acoustic wave propagation in the sample, we fitted the measured thickness distribution by two quadratic curves: setting the x axis parallel to the wedge slope and with $x = 0$ set at the wedge edge, the thickness is fitted as an ellipse $(x - x_0)^2/a^2 + z^2/b^2 = 1$ for the region $20 < x < 120$ μm, and as a parabola $z = cx^2$ for the region $0 < x < 20$ μm (figure 1(b)). Here $x_0 = 170$ μm, $a = 155$ μm, $b = 6.70$ μm, and $c = 0.0042$ μm^{-1}. Further details of the simulation are given in the appendix.

3. Semi-analytical method for acoustic ray trajectories

The theoretical formula for the velocity of a flexural wave, i.e., one that corresponds to the low-frequency approximation for the lowest-order quasi-antisymmetric Lamb mode in a bi-layered plate, is (Shuvalov *et al* 2005)

$$c_f = \sqrt{\sqrt{\frac{\chi}{\rho}}\,\omega d}\,, \tag{1}$$

where $d = d_1 + d_2$ is the total thickness of the plate composed of Au (1) and SiN (2), $\rho = \left(\rho_1 d_1 + \rho_2 d_2\right)/d$ is the average density of the plate, and $\chi = \frac{1}{12d}\left[\frac{\sigma_1 d_1^3 + \sigma_2 d_2^3}{d^2} + 3\frac{\sigma_1\sigma_2 d_1 d_2}{\sigma_1 d_1 + \sigma_2 d_2}\right]$. Here the notation σ_i is introduced for the so-called flexural modulus, $\sigma_i \equiv E_i/(1 - \nu_i^2)$, where E_i denotes the Young modulus and ν_i the Poisson ratio. It is instructive to rewrite equation (1) in the classical form (Graff 1975, Biryukov *et al* 1995)

$$c_f = \sqrt{\sqrt{\frac{\sigma_1}{12\rho_1}}\,\omega d_e}, \tag{2}$$

where, however, in contrast with the case of a single-layer plate, the effective thickness of the composite bi-layered plate d is introduced:

$$d_e = d_1\sqrt{\frac{1+\frac{\sigma_2 d_2^3}{\sigma_1 d_1^3}+3\left(1+\frac{d_2}{d_1}\right)^2\frac{\sigma_2 d_2}{\sigma_1 d_1+\sigma_2 d_2}}{1+\frac{\rho_2 d_2}{\rho_1 d_1}}}.$$

In our experiments the effective thickness of the gold layer and, consequently, the velocity of the flexural wave, depend on the distance from the edge of the gold layer, i.e., $d_1 = d_1(x)$ and $c_f = c_f(x)$. To apply the theory of waves in linear wedges to our case, we approximate our wedge profile by a series of linear segments. At a position x inside a short segment between x_N and $x_{N+1} = x_N + \Delta x$, the effective thickness d_e can be written as $d_e(x) \simeq d_e(x_N) + \frac{\partial d_e}{\partial x}\Delta x \equiv a_N + b_N \Delta x$.

For our sample, flexural waves at frequencies ~100 MHz can be accurately treated in the framework of geometrical acoustics, i.e., ray acoustics. Geometrical acoustics, or the Wentzel, Kramers, Brillouin (WKB) approximation, is theoretically valid when the quantity $|\nabla k|/|\boldsymbol{k}|$, a measure of variation of the wave vector on spatial scales corresponding to the inverse wave vector, is much smaller than the wave vector $|\boldsymbol{k}|$ itself, i.e., when $|\nabla k|/|k|^2 \ll 1$ (Brekhovskikh and Godin 1990, Kravtsov and Orlov 1990). We have verified that this condition holds in our sample not only at 80.4 MHz but also at other detectable frequencies. However, the condition $kd \leqslant 1$, which ensures that the low-frequency approximation equation (1) for the lowest-order quasi-antisymmetric Lamb mode is valid, is not satisfied when the frequency is large compared with 80.4 MHz. The trajectories of the acoustic rays on the (x, y) plane can be obtained from the relations

$$k_x^2 + k_y^2 = k^2, \qquad \frac{dy}{dx} = \frac{k_y}{k_x}, \tag{3}$$

where the flexural wave velocity depends only on one of the following two coordinates: the wave number of the flexural wave $k = k(x) \equiv \omega/c_f(x)$ or its x-component $k_x(x) = \sqrt{k^2(x) - k_y^2}$, which are coordinate-dependent. In contrast, k_y is a constant depending on the starting point of the ray (x_0, y_0). In our experimental geometry, where the laser radiation is focused to a line on the x-axis ($y = 0$), the acoustic waves are emitted in the $\pm y$ directions (except near the ends of the line source): $y = 0$, $k_x(x_0, y = 0) = 0$, and $k_y(x_0, y = 0) = \pm\,\omega/c_f(x_0)$. The integration of equation (3) with these boundary conditions gives ray trajectories in the general form

$$y = \pm\int_{x_0}^{x}\frac{dx'}{\sqrt{\left(c_f(x_0)/c_f(x')\right)^2 - 1}}. \tag{4}$$

The integration of equation (4) provides an analytical expression for the ray trajectories corresponding to starting points (x_0, y_0) in the segment between x_N and x_{N+1}:

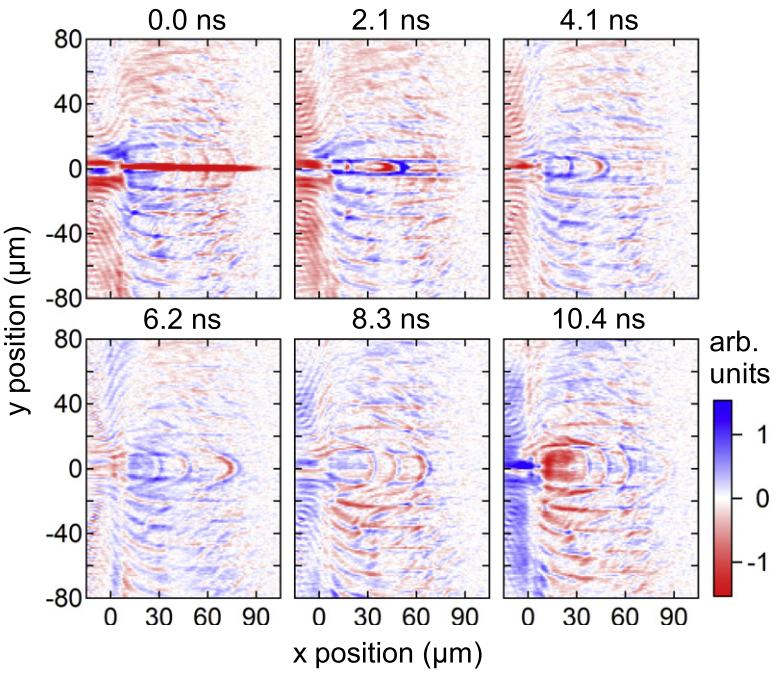


Figure 2. Time-resolved imaging results. The plotted area is indicated in figure 1(a). The image colour represents the z-directed surface velocity.

$$y = \pm\left(x_0 + \frac{b_N}{a_N}\right)\left(\sqrt{\frac{x_0 - x}{x_0 + b_N/a_N}} + \arcsin\sqrt{\frac{x_0 - x}{x_0 + b_N/a_N}}\right). \tag{5}$$

In our experiment, $d_e(x)$ is a monotonically increasing function of x, and the ray trajectories from the source (x_0, $y_0 = 0$) always bend to the $-x$-direction and connect to the next smaller -x segment. For trajectories through the point (x_N, $\pm y_N$) on the segment boundary, the ray trajectory for the next segment is given by

$$y = \pm\left(x_N + \frac{b_{N-1}}{a_{N-1}}\right)\left(\sqrt{\frac{x_N - x}{x_N + b_{N-1}/a_{N-1}}} + \sin^{-1}\left(\sqrt{\frac{x_N - x}{x_N + b_{N-1}/a_{N-1}}}\right)\right) \mp y_N. \tag{6}$$

By repeating this calculation (of equation 6) in each segment with a small enough Δx, semi-analytical acoustic ray trajectories can be obtained. These analytical predictions are compared with our experimental results in the next section.

4. Results

Figure 2 shows some representative experimental acoustic images, which show the out-of-plane velocity of the surface at different delay times. (Animations of the experimental acoustic images are given in the supplementary data, available at stacks.iop.org/njp/16/103029/mmedia.) These images are made up of a superposition of ripples from flexural waves generated by a pump-pulse train of period 12.44 ns. The horizontal central red line on the 0.0 ns image shows where the pump light is focused. Ripples propagating up and down on the images from this thermoelastic line source are clearly visible. These waves include both quasi-symmetric and

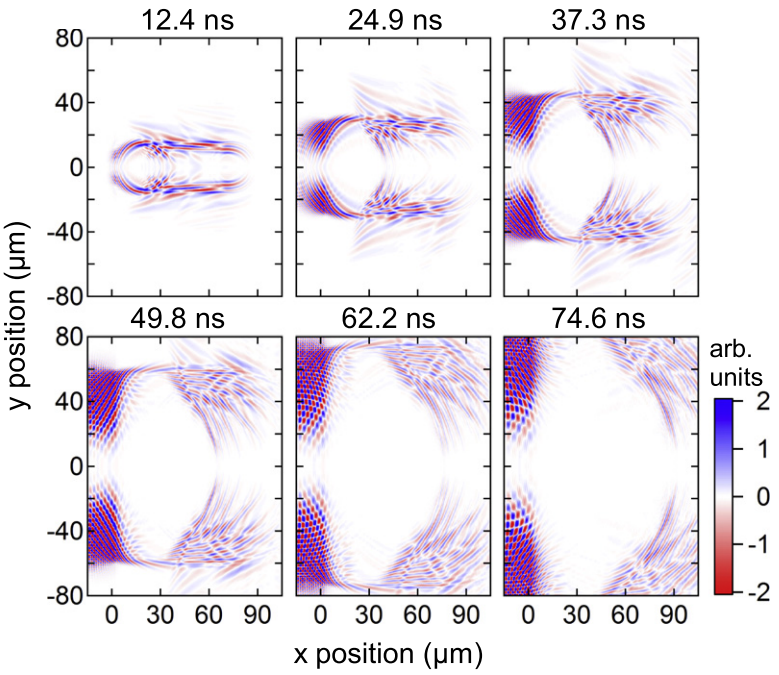


Figure 3. Time-resolved images corresponding to the simulations. The plotted area is indicated in figure 1(a). The image colour represents the z-directed surface velocity.

quasi-antisymmetric Lamb-wave modes, and the strongest wave mode is the zeroth-order quasi-antisymmetric mode, i.e., the flexural wave, which is identified by its approximate propagation velocity of $\sim 1200\,\mathrm{m\,s^{-1}}$ for our frequency range, as derived by following ripples in the time domain. As expected, the wave fronts bend toward the edge of the wedge. Other ripples propagate with components in the $+x$-direction with parabolic-like wave fronts. Since these ripples travel much faster ($\sim 2300\,\mathrm{m\,s^{-1}}$) than the dominant ripples, we identify them as zeroth-order quasi-symmetric Lamb waves, because their velocities agree with that of the S0 guided mode with the velocity $v_l = \sqrt{E_1/\rho_1(1-\nu_1^2)}$ of a free gold plate. The gold film area and the SiN area have opposite image contrast. We presume this difference to be caused by multiple optical reflections inside the transparent SiN slab.

Figure 3 shows acoustic images at different times obtained from the numerical simulations. These images also represent out-of-plane (z-direction) surface velocities to match the experimental results. (Animations of the simulated acoustic images are given in the supplementary data, available at stacks.iop.org/njp/16/103029/mmedia.) In contrast to the experimental images which are generated by a pump-pulse train, the simulated images exhibit ripples generated by a single pump pulse. The amplitude of the simulated ripples in the SiN area is bigger than in the gold wedge area because of the smaller thickness and the mass of the former. In contrast, the amplitude of the ripples in the SiN area in the experimental images are smaller than in the gold wedge area, because the probe-beam reflectance for the SiN is much lower than that for gold. (Our data collection is weighted by the probe-beam power.)

To better understand the behaviour of the different acoustic modes, we calculated temporal Fourier transforms of the set of 24 experimental images (some of which are shown in figure 2) that cover one period of the laser pulses (12.44 ns). We also carried out the same analysis for the 286 simulation images (some of which are shown in figure 3) that cover a time corresponding to

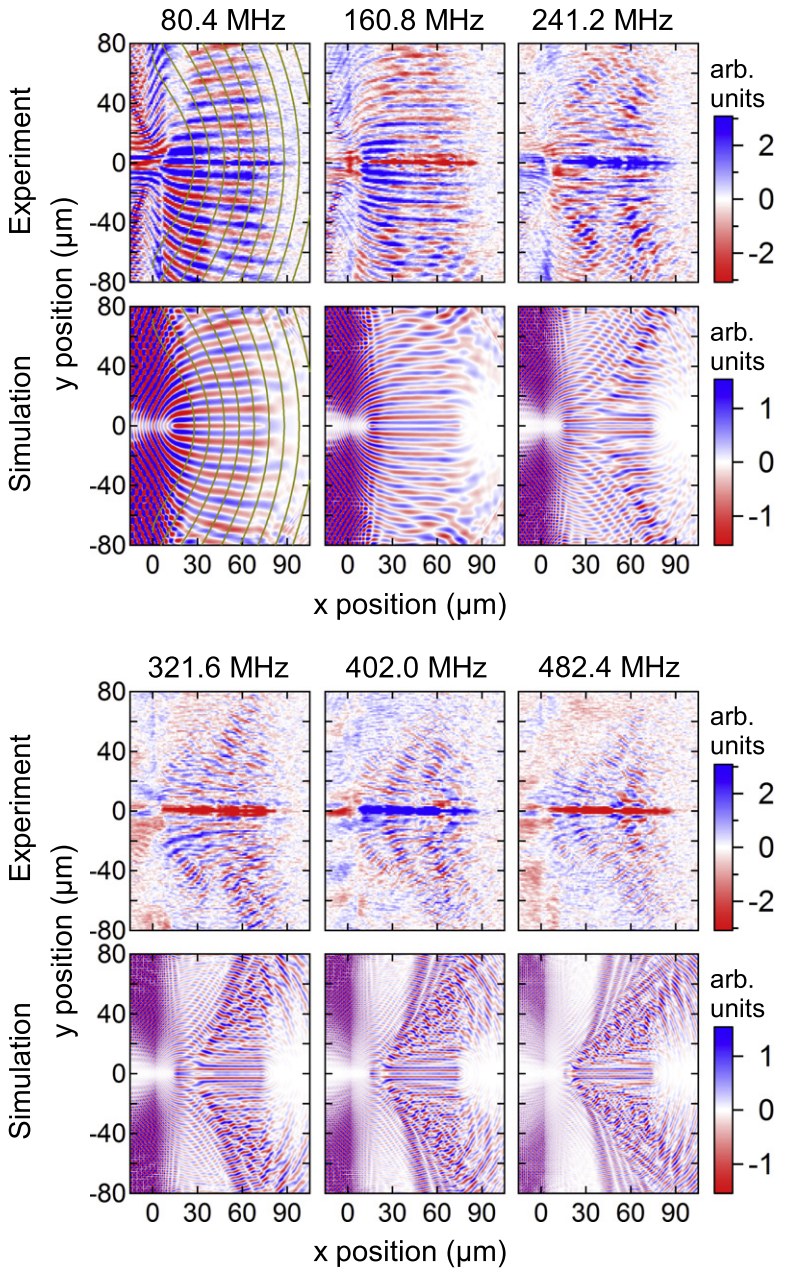


Figure 4. Constant-frequency images corresponding to the simulations. The image colour represents the z-directed surface velocity. The lines on the 80.4 MHz images are the acoustic ray trajectories obtained from the semi-analytical theory.

eight periods of the laser pulses (99.1 ns) in our experiment. Figure 4 shows the thus-obtained constant-frequency acoustic images for both the experiment and the simulation. (Animations of the constant-frequency acoustic images at 80.4 MHz, 160.8 MHz, 241.2 MHz, 321.6 MHz, 402.0 MHz, and 482.4 MHz from both the experiment and the simulation—shown side by side —are given in the supplementary data, available at stacks.iop.org/njp/16/103029/mmedia.) Low-frequency images at 80.4 MHz and 160.8 MHz show strong energy-propagating directions in the $\pm y$ directions, but for higher frequencies these change to the to upper- and lower-right

diagonal directions. The semi-analytical acoustic ray trajectories, calculated according to equations (5) and (6) with the segment width $\Delta x = 0.5\ \mu$m, are plotted on the 80.4 MHz images. These ray trajectories are found to be perpendicular to all wave fronts in both the experimental and simulated images, thus demonstrating the applicability of the ray theory for this frequency.

5. Conclusion

We have imaged propagating near-gigahertz flexural waves in the time-domain in microscopic gold wedges deposited on thin silicon nitride slabs by an ultrafast optical technique. The optical pump pulses are focused to a line source set perpendicular to the edge of the wedge. We observe wave-front bending, especially at low frequencies. This behaviour is explained with the help of an analytical model based on the theory of flexural wave propagation in a bi-layer film and on geometrical acoustics, and is reproduced with numerical simulations. This work should stimulate further studies on the propagation of waves in wedges. Other opto-acoustic experimental methods appropriate for probing or imaging unsupported thin films, such as Brillouin scattering (Grimsditch *et al* 1987, Cuffe *et al* 2012) or Impulsive Stimulated Thermal Scattering (Rogers and Nelson 1994, Rogers *et al* 2000), would be interesting to apply to flexural waves in wedges.

Appendix. Simulation method

For numerical simulations we implement a time-domain finite-element technique (PZFlex, Weidlinger Associates, Inc.). The applied model uses the fitted gold-wedge thickness described previously on a 100 nm thick SiN slab. Both the gold and silicon nitride are treated as isotropic, and we use literature values of physical constants ($\rho_1 = 19300\ \mathrm{kg\,m^{-3}}$, $c_{l1} = 3584\ \mathrm{m\,s^{-1}}$, $c_{t1} = 1207\ \mathrm{m\,s^{-1}}$, $\rho_2 = 2650\ \mathrm{kg\,m^{-3}}$, $c_{l2} = 8311\ \mathrm{m\,s^{-1}}$, and $c_{t2} = 5283\ \mathrm{m\,s^{-1}}$, where c_l is longitudinal wave velocity and c_t is transverse wave velocity) (Anderson 1965). To decrease computing time and memory size, the calculated region 120 μm × 80 μm is applied by incorporation of symmetric boundary conditions that cut through the centre of the line source. The calculation region is continued in the region $x < 0$ for a further 15 μm of SiN slab without gold film to reduce the effect of acoustic reflections from boundaries. On the outer boundaries absorbing boundary conditions are applied. The thermoelastic laser excitation is represented by a simplified model that makes use of a dipole-type horizontal force (y-directed force) with a spatial distribution given by $y\, e^{-y^2/d^2}$ applied over the line source region with length 60 μm, where $d = 1\ \mu$m. The temporal variation of the excitation is chosen as a Gaussian function with a 1 ns $1/e$ full-width-at-half-maximum width. A sufficiently long calculation time (~100 ns, which is 8 times longer than the laser repetition period) is chosen for the simulation. The results of the simulation are compared with our experimental results in the main text.

References

Lagasse P E, Mason I M and Ash E A 1973 *IEEE Trans. Microw. Theory Tech.* **21** 225
De Billy M and Hladky-Hennion A 1999 *Ultrasonics* **37** 413
Shuvalov A and Krylov V 2000 *J. Sound Vib.* **237** 427
Yang C-H and Tsen C-Z 2006 *IEEE Trans. Ultrasonics, Ferroelectr. Freq. Control* **53** 754

Moss S, Maradudin A and Cunningham S 1973 *Phys. Rev.* B **8** 2999
Krylov V V 1998 *J. Acoust. Soc. Am.* **103** 767
Lomonosov A M, Hess P and Mayer A P 2012 *Appl. Phys. Lett.* **101** 031904
Bertoni H and Tamir T 1975 *IEEE Trans. Sonics Ultrason.* **22** 415
Manneberg O, Svennebring J, Hertz H M and Wiklund M 2008 *J. Micromech. Microeng.* **18** 095025
Bayod J J 2011 *J. Vib. Acoust.* **133** 061003
Bowyer E, O'Boy D, Krylov V V and Horner J L 2012 *Appl. Acoust.* **73** 514
Joosse P, Blanch M, Dutton A, Kouroussis D, Philippidis T and Vionis P 2002 *J. Sol. Energy Eng.* **124** 446
Liu I H and Yang C H 2010 *Proc. 2010 IEEE Int. Ultrason. Symp.* p 817
Tung P H and Yang C H 2010 *Proc. 31st Symp. on Ultrasonic Electronics* 31, p 489
Krylov V V and Tilman F 2004 *J. Sound Vib.* **274** 605
Krylov V V and Winward R 2007 *J. Sound Vib.* **300** 43
Krylov V V and Pritchard G V 2007 *Appl. Acoust.* **68** 97
Jia X and De Billy M 1992 *Appl. Phys. Lett.* **61** 2970
Hess P, Lomonosov A M and Mayer A P 2014 *Ultrasonics* **54** 39
Jia J, Shen Z, Wang L and Yuan L 2011 *Chin. Opt. Lett.* **9** 022501
Edwards R S, Dutton B and Clough A 2012 *Appl. Phys. Lett.* **100** 184102
Sugawara Y, Wright O, Matsuda O, Takigahira M, Tanaka Y, Tamura S and Gusev V 2002 *Phys. Rev. Lett.* **88** 185504
Tachizaki T, Muroya T, Matsuda O, Sugawara Y, Hurley D H and Wright O B 2006 *Rev. Sci. Instrum.* **77** 043713
Shuvalov A L, Poncelet O, Deschamps M and Baron C 2005 *Wave Motion* **42** 367
Graff K 1975 *Wave Motion in Elastic Solids* (New York: Dover Publications)
Biryukov S V, Gulyaev Y V, Krylov V V and Plessky V P 1995 *Surface Acoustic Waves in Inhomogeneous Media* vol 20 (Berlin: Springer)
Brekhovskikh L M and Godin O A 1990 *Acoustics of Layered Media I: Plane and Quasi-plane Waves* (Berlin: Springer)
Kravtsov Y A and Orlov Y I 1990 *Geometrical Optics of Inhomogeneous Media* (Berlin: Springer)
Grimsditch M, Bhadra R and Schuller I K 1987 *Phys. Rev. Lett.* **58** 1216
Cuffe J, Chavez E, Shchepetov A, Chapuis P-O, El Boudouti E H, Alzina F, Kehoe T, Gomis-Bresco J, Dudek D, Pennec Y *et al* 2012 *Nano Lett.* **12** 3569
Rogers J A and Nelson K A 1994 *J. Appl. Phys.* **75** 1534
Rogers J A, Maznev A A, Banet M J and Nelson K A 2000 *Ann. Rev. Mater. Sci.* **30** 117
Anderson O L 1965 *Physical Acoustics* vol III, Part B ed W P Mason (New York: Academic)